



ELSEVIER

Available online at [www.sciencedirect.com](http://www.sciencedirect.com)

 ScienceDirect

Proceedings of the Combustion Institute 31 (2007) 1973–1981

Proceedings  
of the  
Combustion  
Institute

[www.elsevier.com/locate/proci](http://www.elsevier.com/locate/proci)

# Laser induced fluorescence of formaldehyde and Raman measurements of major species during partial catalytic oxidation of methane with large H<sub>2</sub>O and CO<sub>2</sub> dilution at pressures up to 10 bar <sup>☆</sup>

Adrian Schneider, John Mantzaras <sup>\*</sup>, Rolf Bombach,  
Sabine Schenker, Niclas Tylli, Peter Jansohn

*Paul Scherrer Institute, Combustion Research, CH-5232 Villigen PSI, Switzerland*

## Abstract

The catalytic partial oxidation (CPO) of CH<sub>4</sub>/O<sub>2</sub> mixtures diluted with large amounts of H<sub>2</sub>O and CO<sub>2</sub> (up to 43% and 21% vol., respectively) was investigated experimentally and numerically in the pressure range 4 bar ≤ *p* ≤ 10 bar. Experiments were carried out in an optically accessible channel-flow catalytic reactor coated with Rh/ZrO<sub>2</sub>, and included planar laser induced fluorescence (LIF) of formaldehyde for the assessment of homogeneous (gas-phase) ignition and one-dimensional spontaneous Raman measurements of all major gas-phase species for the evaluation of the heterogeneous (catalytic) processes. Simulations were performed with a full elliptic model that included detailed heterogeneous and homogeneous chemical reaction schemes. Over the reactor length with negligible gas-phase chemistry contribution, the employed heterogeneous reaction scheme provided good agreement to the measured methane consumption and synthesis gas yields, overpredicting mildly the partial over the total oxidation route. It was shown that the added water provided a source of O(s) and OH(s) surface radicals that enhanced the methane conversion and H<sub>2</sub> yields and reduced the CO yields. Moreover, the addition of CO<sub>2</sub> had a negligible chemical effect on the aforementioned parameters. An increase in pressure from 4 to 10 bar had a minor impact on the methane conversion and hydrogen selectivity. The employed gaseous scheme reproduced the LIF-measured onset of homogeneous ignition, although it underpredicted the extent of the formaldehyde zone ahead of the flame and the flame propagation characteristics at the highest investigated pressure (10 bar).

© 2006 The Combustion Institute. Published by Elsevier Inc. All rights reserved.

**Keywords:** Catalytic partial oxidation of methane; Laser induced fluorescence of formaldehyde; In situ Raman measurements; Exhaust gas dilution

## 1. Introduction

The catalytic partial oxidation (CPO) of methane to synthesis gas can be accomplished autothermally and selectively at millisecond contact times over noble metals [1,2], rendering this

<sup>☆</sup> Supplementary data for this article can be accessed online. See Appendix A.

<sup>\*</sup> Corresponding author. Fax: +41 56 3102199.

E-mail address: [ioannis.mantzaras@psi.ch](mailto:ioannis.mantzaras@psi.ch) (J. Mantzaras).

process particularly attractive for on-board fuel reforming in many practical devices such as fuel-cells [3], internal combustion engines [4] and natural-gas-fired turbines [5]. In the last two applications, a fraction of the hydrocarbon fuel undergoes CPO and the produced synthesis gas allows for enhanced stability of the follow-up flame. To advance these new combustion technologies, Appel et al. [6] have recently investigated CPO of  $\text{CH}_4/\text{air}$  over  $\text{Rh}/\text{ZrO}_2$  at a moderate pressure of 6 bar. Therein, in situ one-dimensional (1-D) Raman measurements of gas-phase species concentrations were used, in conjunction with detailed simulations, to elucidate the underlying hetero-/homogeneous processes.

In the last years, the CPO of natural-gas/air mixtures diluted with large recycled exhaust gas has received increased attention in power generation. One such example is the advanced zero emissions power process [7], wherein the recycled  $\text{H}_2\text{O}$  and  $\text{CO}_2$  comprise up to 80% of the feed. The addition of water is beneficial in many CPO-based chemical processes: it facilitates the autothermal reforming of methane [8] and ethanol [9], and it suppresses the formation of olefins in the reforming of higher hydrocarbons [10]. Understanding the impact of large  $\text{H}_2\text{O}/\text{CO}_2$  dilution on the hetero-/homogeneous processes during CPO of methane (the main component of natural gas) is of paramount importance for power systems with exhaust recirculation.

The present study undertakes an experimental and numerical investigation of methane CPO with large  $\text{H}_2\text{O}$  and  $\text{CO}_2$  dilution (up to 43% and 21% vol., respectively) that is relevant to power generation cycles. High-pressure experiments (up to 10 bar) were carried out in an optically accessible reactor. In situ 1-D Raman measurements of major species concentrations were used to assess the heterogeneous processes and planar laser induced fluorescence (LIF) of formaldehyde monitored gaseous combustion. The main objectives were to investigate the impact of  $\text{H}_2\text{O}$  and  $\text{CO}_2$  on the methane consumption and product selectivities at power-generation-relevant conditions, to establish an experimental technique for the assessment of homogeneous ignition during CPO, and to provide validated hetero-/homogeneous chemical reaction schemes at high pressures.

## 2. Experimental

### 2.1. Test rig and catalyst preparation

Experiments were carried out in an optically accessible catalytic channel-flow reactor, positioned inside a high-pressure cylindrical tank (Fig. 1). The reactor comprised two non-porous  $\text{Si}[\text{SiC}]$  ceramic plates (300 mm long, 104 mm

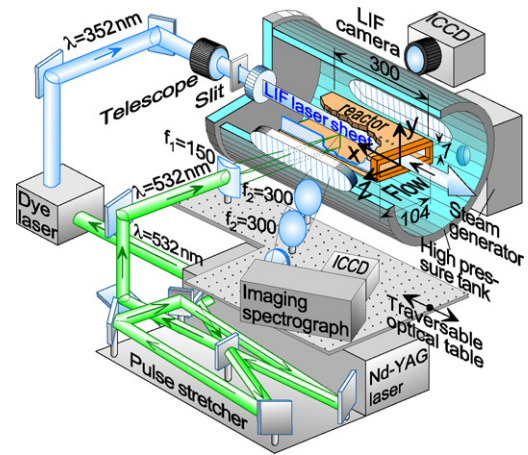


Fig. 1. Schematic of the reactor and the Raman/LIF set-up.

wide, placed 7 mm apart) and two 3-mm-thick quartz windows. A  $\text{Rh}/\text{ZrO}_2$  coating (2% wt. Rh) was applied to the inner  $\text{Si}[\text{SiC}]$  surfaces. The surface temperatures were monitored by thermocouples (12 for each plate) arranged along the  $x$ - $y$  symmetry plane and embedded 0.9 mm beneath the catalyst through holes eroded from the outer  $\text{Si}[\text{SiC}]$  surfaces. Two 350-mm-long and 35-mm-thick quartz windows on the high-pressure tank maintained optical access from both reactor sides. Two additional quartz windows, one at the rear flange of the tank and the other (not shown in Fig. 1) at the reactor exit, provided a further streamwise optical access for the LIF excitation beam. Details of the reactor/tank assembly have been provided elsewhere [6,11,12].

Pure oxygen was used in the feed with nitrogen added as balance. Superheated steam was supplied by an AWTEC-DLR steam-generator. The  $\text{O}_2$ ,  $\text{N}_2$  (and  $\text{CO}_2$  when applicable) flows were mixed and then electrically preheated. Room-temperature  $\text{CH}_4$  and superheated steam were injected downstream; the feed achieved a good degree of premixedness in two sequential static mixers and a 30-mm-long packing of 2-mm-diameter ceramic spheres. The mixture was finally driven into the reactor through a 50-mm-long inert honeycomb. A thermocouple positioned at the downstream end of the honeycomb provided the inlet temperature of the feed.

The catalyst preparation involved incipient wetness impregnation of the  $\text{ZrO}_2$  support with a  $\text{Rh}(\text{NO}_3)_3$  solution. The impregnated catalyst powder was calcined at 600 °C for 5 h. A slurry created from the catalyst powder and a solvent mixture was sprayed on the  $\text{Si}[\text{SiC}]$  plates, yielding a 12- $\mu\text{m}$ -thick coating. The coated  $\text{Si}[\text{SiC}]$  plates were subsequently calcined at 600 °C for 1 h. BET ( $\text{N}_2$  physisorption) and CO chemisorption were used to assess the total and active surface

areas, respectively. The deduced ratio of the active to geometrical area in the tested samples was 4.5. Post-combustion X-ray photoelectron spectroscopy (XPS) analysis indicated that bulk elements (e.g., Si) did not diffuse to the surface. The catalyst was reduced in a heated (400 °C) flow of H<sub>2</sub>/N<sub>2</sub> before each combustion test.

## 2.2. Laser diagnostics

The Raman/LIF set-up is depicted in Fig. 1. A traversable mirror directed the frequency-doubled 532 nm radiation of an Nd:YAG pulsed laser (Quantel YG981E20-CL, 380 mJ pulse energy, 12 ns pulse) to the Raman or to the LIF set-up. In the Raman experiments, the 532 nm beam was temporally stretched to 34 ns using a partially reflecting mirror and an optical delay line for the transmitted radiation (Fig. 1). This allowed for efficient use of the entire pulse energy without window damage or dielectric gas breakdown. The temporally stretched and expanded (25 mm diameter) beam was focused through the tank and reactor side-windows into a vertical line (~0.3 mm thick) by an  $f_1 = 150$  mm cylindrical lens. The focal line spanned the 7-mm transverse gap and was laterally offset ( $z = 15$  mm) to increase the light collection angle and minimize thermal beam steering [11,13]. Two  $f_2 = 300$  mm spherical lenses focused the scattered light to the entrance slit of a 25 cm imaging spectrograph (Chromex-250i). The dispersed light was recorded on an intensified CCD camera (Princeton Instruments MAX-1024HQ, 1024 × 254 pixels). To increase the spatial resolution, only the upper channel half-height was recorded. Each image comprised 630 × 254 pixels that corresponded to wavelength and transverse ( $y$ ) distance, respectively. The 3.5 mm half-height was resolved with 200 pixels, which were further binned to 84 pixels. A holographic notch-filter (Kaiser HNPf-532.0-1.5) and a colored glass filter were placed before the spectrograph slit to attenuate the scattered Rayleigh signal and the stray laser light. The spectral dispersion extended up to 4500 cm<sup>-1</sup>, allowing observation of all major species. Given the steady operating conditions, 2000 images were averaged to increase the signal-to-noise ratio. The effective Raman cross-sections were evaluated by recording the signals of several pressurized CH<sub>4</sub>, N<sub>2</sub>/H<sub>2</sub> and CO<sub>2</sub> containing mixtures, air, and the actual feed mixture. Those tests also quantified the cross-talk between the CO<sub>2</sub>/O<sub>2</sub> and CO/N<sub>2</sub>. Spectroscopic data for the CH<sub>4</sub>, H<sub>2</sub>O, CO<sub>2</sub> and CO Raman cross-sections were obtained from Refs. [14–16]. Measurements were acquired at 14 mm ≤  $x$  ≤ 168 mm by traversing axially an optical table that supported both sending and collecting optics (Fig. 1). Raman data closer than 0.3 mm to the upper wall were discarded due to low signal-to-noise ratio.

At fuel-rich conditions, planar LIF of OH is not amenable due to the associated sub-ppm levels [6]. Formaldehyde LIF was thus introduced, whereby the 532 nm radiation pumped a tuneable dye laser (Quantel TDL90 NBP2UVT3) filled with pyridine-1 dye. Its frequency-doubled radiation at 352 nm was transformed into a slightly diverging laser sheet (propagating counterflow along the  $x$ - $y$  symmetry plane, Fig. 1) by a telescopic system. The broadband fluorescence was collected at 90° with an intensified CCD camera (LaVision-IRO with 1392 × 1024 pixels, recorded with a binning of 2 × 2). The collection optics included achromatic lenses and filters that provided spectral detection between 410 and 480 nm. Zones of 110 × 7 mm<sup>2</sup> were recorded on a 696 × 44 pixel section, and the camera was traversed axially to map the entire reactor extent. Uncertainties in the broadband emission of formaldehyde and the significant laser radiation absorption along its propagation path (given the large amounts of CH<sub>2</sub>O) precluded quantification of the LIF signals. The present study reports the first direct measurements of homogeneous ignition in CPO using CH<sub>2</sub>O-LIF. In catalytic systems, this technique has only been used to measure the pure heterogeneous production of formaldehyde in the oxidation of methanol over Pt [17] at low temperatures (140 °C).

## 3. Numerical

A full elliptic 2-D CFD code [13,18] provided the simulation platform. It included the multi-step heterogeneous scheme of Deutschmann [19], comprising 38 reactions, 12 surface and 6 gaseous species. The impact of added radical (OH, H, O) adsorption/desorption reactions [20] (not included in the original scheme [19]) on homogeneous ignition was minimal. For gas-phase chemistry, the C<sub>2</sub>/H/O mechanism of Warnatz et al. [21] (164 reversible reactions and 34 species, with appropriate pressure dependencies for six reactions) was employed. Transport was modeled with mixture-average diffusion including thermal diffusion for the light species, using the CHEMKIN database [22]. Gaseous and surface chemical reaction rates were evaluated with CHEMKIN [23] and Surface-CHEMKIN [24], respectively. Gas-phase and surface thermochemical data were included in the provided mechanisms.

Uniform properties for the temperature, the axial velocity and the species mass fractions were used at the inlet. Fitted curves through the 12 thermocouple measurements of each plate provided the interfacial energy boundary conditions at  $y = 0$  and 7 mm, respectively. No-slip conditions for both velocity components were applied at the channel walls and zero-Neumann conditions at the outlet. An orthogonal staggered mesh of

480 × 84 points (over the 300 and 7 mm dimensions, respectively) was sufficient to produce a grid-independent solution.

#### 4. Results and discussion

The experimental conditions are provided in Table 1. The minimum flow rate requirements of the steam-generator placed a lower limit to the inlet Reynolds numbers, which ranged from 2500 to 2650 (based on the 13.1 mm channel hydraulic diameter). The flow could be treated as laminar since recent turbulent catalytic combustion studies [25] have shown that the strong flow laminarization induced by the heat transfer from the hot walls guaranteed laminar flow conditions even at considerably higher inlet Reynolds numbers.

##### 4.1. Heterogeneous processes

Comparisons between Raman-measured and predicted species transverse profiles are illustrated in Figs. 2–4. For clarity, up to 20 of the total 84 measuring points are provided over the experimentally resolved extent  $0 \leq y \leq 3.2$  mm. The measurement accuracy was  $\pm 3\%$  for species compositions  $\geq 10\%$  vol. and  $\pm 10\%$  for compositions as low as 0.5% vol.; concentrations less than 0.5% vol. entailed larger measurement uncertainties. The resulting C/H/O element balances along the channel were reproduced within 5%. Figure 5 provides the computed streamwise profiles of the average (over the 7 mm channel height) species mole fractions and the thermocouple-measured upper and lower wall temperatures for Cases 2 and 5. The temperature differences between the two walls were within 25 K. Emphasis is placed on the pure H<sub>2</sub>O dilution cases since, as shown next, CO<sub>2</sub> had a minor chemical impact.

Homogeneous ignition was attained in all cases of Table 1 as evidenced by the formaldehyde LIF (see forthcoming Fig. 8). Streamwise profiles of the computed catalytic and gas-phase species production rates (the latter integrated over the 7 mm channel-height) are provided in Fig. 6 for Cases 2

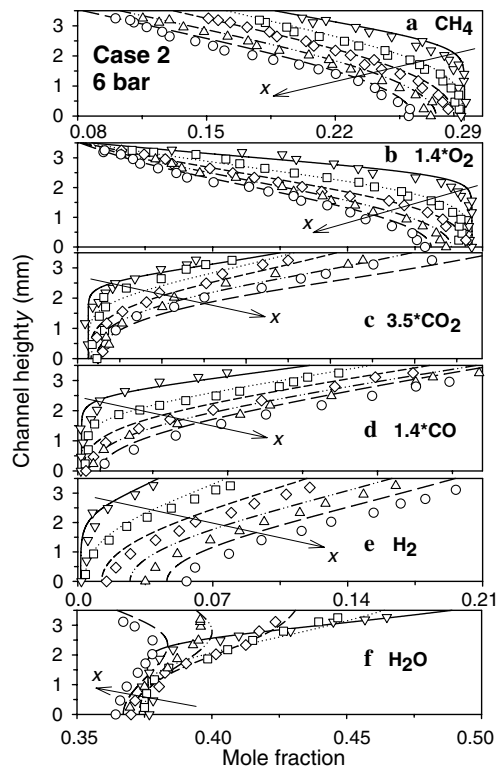


Fig. 2. Predicted (lines) and measured (symbols) profiles of species mole-fraction for Case 2:  $x = 14$  mm (solid-lines, lower-triangles),  $x = 48$  mm (dotted-lines, squares),  $x = 88$  mm (short-dashed-lines, diamonds),  $x = 128$  mm (double-dotted-dashed lines, upper-triangles),  $x = 168$  mm (long-dashed-lines, circles). The wall is at  $y = 3.5$  mm and the symmetry plane at  $y = 0$ .

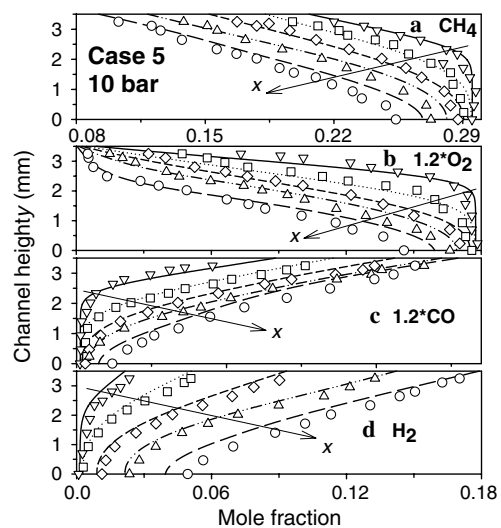


Fig. 3. Measured and predicted species profiles for Case 5. The notation follows Fig. 2.

Table 1  
Experimental conditions<sup>a</sup>

Case	$p$	$\varphi$	$T_{IN}$	$U_{IN}$	CH <sub>4</sub>	H <sub>2</sub> O	CO <sub>2</sub>
1	4	2.5	457	1.72	20	42	—
2	6	4.0	566	1.62	29	38	—
3	8	2.5	569	1.07	20	43	20
4	10	2.5	553	0.82	21	42	21
5	10	4.0	549	0.93	30	37	—

<sup>a</sup> Inlet properties ( $p$  in bar,  $T_{IN}$  in K,  $U_{IN}$  in m/s) and %vol. feed composition. Case 1 has also 22% vol. CO. O<sub>2</sub> is deduced from the equivalence ratio ( $\varphi$ ) and the balance is N<sub>2</sub>.

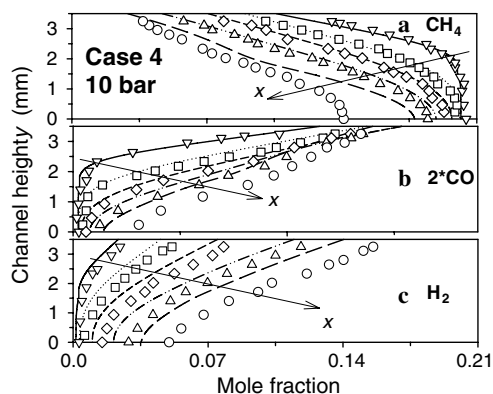


Fig. 4. Measured and predicted species profiles for Case 4. The notation follows Fig. 2.

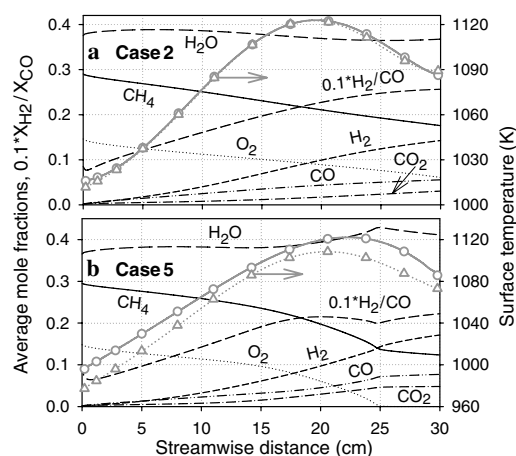


Fig. 5. Computed streamwise profiles of  $y$ -averaged species mole fractions. Streamwise profiles of wall temperatures (gray lines) fitted through the thermocouple measurements (circles: upper wall, triangles: lower wall). The sharp bends at  $x \approx 25$  cm in (b) are associated with the end of flame (Fig. 8(5b)).

and 5. Gas-phase chemistry was negligible at  $x \leq 120$  mm (Case 2) and  $x \leq 86$  mm (Case 5), wherein its contribution was less than  $\sim 5\%$  of the catalytic pathway. Similarly, in Case 4 the computations indicated negligible gas-phase contribution for  $x \leq 80$  mm. Those axial extents corresponded to the first four transverse profiles of Fig. 2 and the first three profiles of Figs. 3 and 4. The predicted onset of homogeneous ignition (defined in Section 4.4 by the formaldehyde rise) was located  $\sim 20$  mm farther downstream of the aforementioned onset of appreciable gas-phase contribution. As further discussed in Section 4.4, the predicted homogeneous ignition distances ( $x_{ig}$ ) were in general agreement with the LIF measurements, suggesting that the above-computed

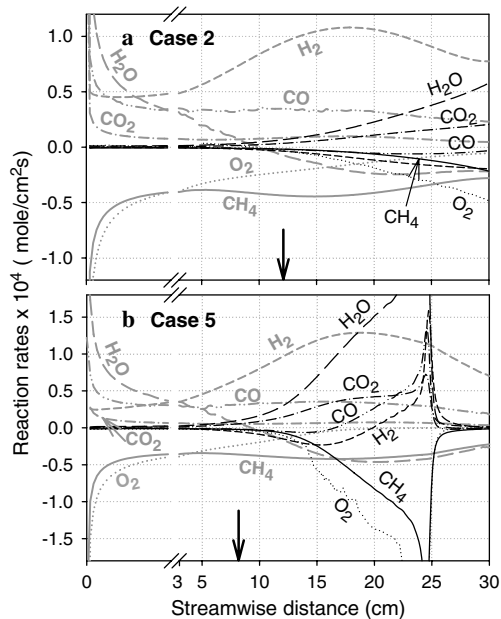


Fig. 6. Computed species production rates (gray lines: catalytic, black lines: gaseous). For clarity, the initial 3 cm are expanded. The thick arrows indicate the position where gas-phase contribution becomes appreciable.

reactor extent with negligible gas-phase contribution was realistic. Over this extent, comparisons between measured and predicted methane mole fractions indicated relative differences of up to 4% (see Figs. 2a, 3a, and 4a), which were well within the experimental uncertainty. Larger differences were only evidenced at the last streamwise distance of Figs. 3 and 4 due to the influence of gas-phase combustion and the associated slower predicted flame propagation (see Section 4.4).

In the  $H_2O$  dilution cases, the partial oxidation products (CO and  $H_2$ ) were somewhat underpredicted (Figs. 2d, e and 3c, d). On the other hand, the total oxidation products ( $CO_2$  and  $H_2O$ ) were slightly overpredicted as shown in Fig. 2 ( $CO_2$  and  $H_2O$  are not provided in Fig. 3, however, the same trends were also observed there). Thus, the employed heterogeneous reaction scheme favored slightly the partial over the total oxidation route and this behavior was in qualitative agreement with earlier  $CH_4$ /air CPO experiments without dilution [6]. Comparisons between measurements and predictions have also attested the aptness of the employed heterogeneous scheme in the presence of  $CO_2$  dilution and further revealed the same small overprediction of the partial over the total oxidation route (see Fig. 4, the first three CO and  $H_2$  profiles). Having established the overall applicability of the employed heterogeneous reaction scheme in the presence of large  $H_2O$

and CO<sub>2</sub> dilution, the following numerical analysis in Sections 4.2 and 4.3 elucidates the underlying catalytic processes.

#### 4.2. Production of synthesis gas

The O<sub>2</sub> profiles in Figs. 2 and 3 indicated a mass-transport-limited catalytic conversion (manifested by the very low O<sub>2</sub> levels at the wall). In the upstream regions of minimal gas-phase pathway participation, there was always O<sub>2</sub> available (Figs. 2b and 3b). In the first ~3 cm of the reactor, the O<sub>2</sub>/CH<sub>4</sub> catalytic destruction ratio ranged between one and two (Fig. 6), demonstrating a strong contribution of complete oxidation (CH<sub>4</sub> + 2O<sub>2</sub> → 2H<sub>2</sub>O + CO<sub>2</sub>) in addition to CPO (2CH<sub>4</sub> + O<sub>2</sub> → 4H<sub>2</sub> + 2CO). Farther downstream, the destruction rate of CH<sub>4</sub> overtook that of O<sub>2</sub>, and the molar ratio H<sub>2</sub>/CO approached two at the end of the catalytically dominant zones (Fig. 5a). The total oxidation at the upstream locations resulted in very steep transverse wall gradients of H<sub>2</sub>O and CO<sub>2</sub> (see the first two profiles in Fig. 2c and f).

Water was catalytically produced at  $x \leq 100$  mm (Fig. 6a) and  $x \leq 92$  mm (Fig. 6b). Farther downstream, the catalyst turned to a sink of H<sub>2</sub>O due to steam reforming (CH<sub>4</sub> + H<sub>2</sub>O → CO + 3H<sub>2</sub>). Moreover, even well-downstream the onset of homogeneous ignition ( $x > x_{ig}$ ), the catalytic pathway continued to play a pivotal role (Fig. 6); therein, the catalyst consumed CH<sub>4</sub> and H<sub>2</sub>O, while it produced H<sub>2</sub>, CO and CO<sub>2</sub>. This was a result of heterogeneously catalyzed steam reforming, which was responsible for H<sub>2</sub>/CO molar ratios approaching three at the reactor exit (Fig. 5a). The catalytic production of CO<sub>2</sub> was due to the water gas shift reaction CO + H<sub>2</sub>O → CO<sub>2</sub> + H<sub>2</sub>. The aforementioned catalytic production or destruction of the major species was also affirmed experimentally by the sign of the Raman-measured transverse gradients near the wall (Figs. 2–4). The pure catalytic methane conversion (before the onset of appreciable gas-phase contribution) was as high as 17%, with a hydrogen selectivity (based on the stoichiometry of the partial oxidation reaction) of up to 85%. Computations at a constant mass throughput and wall temperature (from 900 to 1200 K) have shown that, for methane conversions of up to 50%, an increase in pressure from 4 to 10 bar enhanced only mildly (up to 5%) the CH<sub>4</sub> conversion and the H<sub>2</sub>/CO selectivities. Those findings were in general agreement with lower-pressure experiments (1.4–5.5 bar [26]) of CH<sub>4</sub>/air CPO.

For the present high surface temperatures (Fig. 5), coking was not an issue: post-combustion catalyst examination indicated no visible carbon deposition. While it is understood that non-visible carbon deposition can still influence the catalytic activity, the steady reactor performance suggested that surface carbon did not lead to catalyst deactivation over the timescales of testing.

#### 4.3. Effect of H<sub>2</sub>O and CO<sub>2</sub> dilution on synthesis gas

The impact of water on the synthesis gas yields was investigated numerically by replacing the diluent H<sub>2</sub>O with a fictitious species H<sub>2</sub>O\* that had the same thermodynamic and transport properties as H<sub>2</sub>O but did not participate in any reaction. H<sub>2</sub>O\* simulated only the incoming diluent whereas the catalytic and gaseous pathways were still allowed to generate H<sub>2</sub>O. The surface coverage of Case 2 with H<sub>2</sub>O and H<sub>2</sub>O\* dilution is presented in Fig. 7. The addition of H<sub>2</sub>O increased the H<sub>2</sub>O(s) coverage due to partial equilibration of the H<sub>2</sub>O adsorption/desorption reactions. The higher H<sub>2</sub>O(s) coverage, in turn, enhanced the OH(s) and O(s) coverage (Fig. 7). The reduced impact of the H(s)-consuming reactions H(s) + O(s) = OH(s) + Rh(s) (due to the increased OH(s)/O(s) ratio of the H<sub>2</sub>O- compared to the H<sub>2</sub>O\*-dilution) and H(s) + OH(s) = H<sub>2</sub>O(s) + Rh(s) (due to the corresponding increase in the H<sub>2</sub>O(s)/OH(s) ratio) led to a ~20% increase in H(s) for the former case (Fig. 7) that, in turn, promoted the H<sub>2</sub>-producing desorption reaction 2H(s) → H<sub>2</sub> + 2Rh(s). The addition of H<sub>2</sub>O also caused a significant drop in C(s) (Fig. 7) since the higher O(s) coverage accelerated the C(s)-depleting reaction C(s) + O(s) = CO(s) + Rh(s). The higher amounts of O(s) favored CO(s) + O(s) = CO<sub>2</sub>(s) + Rh(s) against CO(s) → CO + Rh(s),

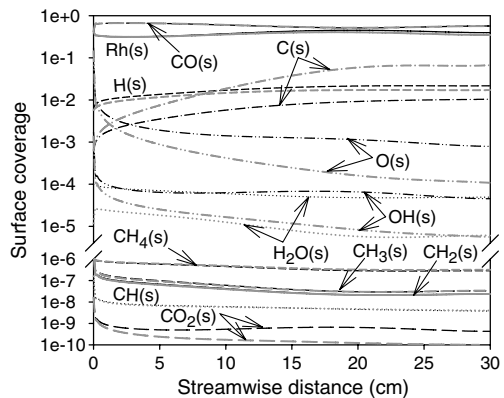


Fig. 7. Surface coverage for Case 2 (black lines) and for the same case with diluent chemically inert H<sub>2</sub>O\* (gray lines).

thus reducing the yields of CO and increasing those of CO<sub>2</sub>. When H<sub>2</sub>O was replaced by H<sub>2</sub>O\*, computations over the reactor extent with negligible gas-phase contribution have shown a 10% decrease in CH<sub>4</sub> conversion, a 21% drop in H<sub>2</sub> yields and a 6% increase in CO yields. This effect of H<sub>2</sub>O dilution is consistent with autothermal CPO experiments [8]; the current computations have provided a first identification of the surface pathways responsible for this behavior.

The effect of CO<sub>2</sub> dilution was investigated similarly through a fictitious species CO<sub>2</sub>\*. The computations revealed that neither the CH<sub>4</sub> conversion nor the H<sub>2</sub>/CO yields were affected by the presence of CO<sub>2</sub>. When CO<sub>2</sub> was replaced by CO<sub>2</sub>\*, the main change was a drop in CO<sub>2</sub>(s) by a factor of five; however, CO<sub>2</sub>(s) was already too low (Fig. 7) to significantly affect the other surface species.

#### 4.4. Homogeneous ignition

The onset of homogeneous ignition is a safety concern in CPO-based high-pressure systems (e.g., turbines). Comparisons between LIF-measured and predicted CH<sub>2</sub>O distributions are illustrated in Fig. 8. Case 1 was specifically included so as to investigate homogeneous ignition at a much higher CO/H<sub>2</sub> ratio. The predicted levels of formaldehyde ranged from 1000 to 4100 ppmv. The flame shapes exhibited small asymmetries due to differences between the two channel wall temperatures (see Fig. 5). The onset of homogeneous ignition ( $x_{ig}$ ), shown with the green arrows in Fig. 8, was defined in both measurements and predictions by the location where the formaldehyde levels rose

to 5% of their maximum flame value. There was an overall good agreement between the measured and predicted  $x_{ig}$  (within 5% for Cases 1, 4 and 5 and within 20% for Cases 2 and 3).

Despite the good homogeneous ignition predictions, there were differences in the spatial distribution of formaldehyde. The predicted formaldehyde was concentrated in thin reaction zones, whereas the measurements indicated a broader distribution in the pre-flame region. The latter was not an experimental artifact as evidenced by the following analysis. Tuning the excitation wavelength off-resonance revealed no significant background signal contribution. This was not surprising, since broadband fluorescing polyaromatic-hydrocarbons (PAH) were only formed downstream the end of the flame at the reactor exhaust (as visibly seen and also as attested by LIF measurements in the exhaust at shallow optical collection angles). An elongation by a factor of two of the apparent formaldehyde zone has been reported in LIF measurements of non-preheated, atmospheric-pressure stoichiometric and slightly rich methane/air flames due to the exaggerated signal contribution of the colder (and hence higher density) zones upstream of the flame and due to quenching variations [27]. However, this effect is diminished in the present experiments due to mixture preheat, moderate flame temperatures (up to 1620 K at the channel center), and small changes of the gas composition (due to the substantially fuel-rich mixtures and the large H<sub>2</sub>O dilution). Formaldehyde is known to form upstream of the flame front [27], however, it appears that the employed reaction scheme underestimates the contribution of those zones. Sensitivity analysis has further indicated that homogeneous ignition was affected by the H<sub>2</sub> and CO adsorption/desorption steps, as they determined the composition of the ignitable gaseous mixture. The small differences between Raman measurements and predictions could induce a ~3% difference in  $x_{ig}$ . This chemistry coupling has nevertheless exemplified the importance of the present combined hetero-/homogeneous investigations.

The measured flame sweep angles (denoted by  $\alpha$  in Fig. 8(5)) were reproduced well by the predictions only at pressures up to 8 bar. In Cases 4 and 5 (10 bar), the measured flame lengths were noticeably shorter than the predicted ones, suggesting that the employed gas-phase scheme underpredicted the propagation characteristics (laminar flame speeds) at those mixture compositions and pressures. However, in practical CPO systems the main requirement on the gas-phase scheme is to capture ignition delay (i.e.,  $x_{ig}$ ) and not propagation characteristics. Despite some apparent deficiencies of the employed reaction scheme, the present study has shown that it can reproduce the key safety issue of homogeneous ignition.

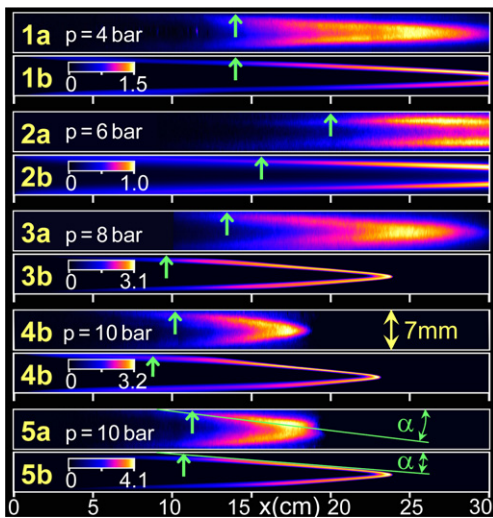


Fig. 8. (a) LIF-measured, and (b) numerically predicted distributions of CH<sub>2</sub>O for the five cases of Table 1. The color bars provide the CH<sub>2</sub>O in ppmv  $\times 10^{-3}$ .

## 5. Conclusions

The partial catalytic oxidation of  $\text{CH}_4/\text{O}_2/\text{H}_2\text{O}/\text{CO}_2/\text{N}_2$  mixtures over  $\text{Rh}/\text{ZrO}_2$  was investigated experimentally with in situ, 1-D Raman and planar  $\text{CH}_2\text{O}$  LIF measurements. Numerical simulations have shown that the employed homogeneous reaction scheme, despite deficiencies in the extent of the formaldehyde zone and its propagation characteristics at 10 bar, reproduced well the onset of homogeneous ignition. The heterogeneous reaction scheme provided good agreement to the synthesis gas yields overpredicting slightly the partial over the total oxidation routes. The addition of  $\text{H}_2\text{O}$  increased the  $\text{CH}_4$  conversion and  $\text{H}_2$  yields and decreased the  $\text{CO}$  yields, due to a corresponding enhancement in the  $\text{O}(\text{s})$  and  $\text{OH}(\text{s})$  surface coverage. An increase in pressure from 4 to 10 bar produced only a small increase in the methane conversion and the  $\text{H}_2/\text{CO}$  selectivities, while the addition of  $\text{CO}_2$  had an overall minimal chemical impact.

## Acknowledgments

Support was provided by the Swiss Federal Office of Energy (BFE) and ALSTOM Power of Switzerland.

## Appendix A. Supplementary data

Supplementary data associated with this article can be found in the online version at doi:10.1016/j.proci.2006.08.076.

## References

- [1] D.A. Hickman, L.D. Schmidt, *AIChE* 39 (1993) 1164–1177.
- [2] O. Deutschmann, L.D. Schmidt, *AIChE* 44 (1998) 2465–2477.
- [3] A.K. Chaniotis, D. Poulidakos, *J. Power Sources* 142 (2004) 184–193.
- [4] T. Allgeier, M. Klenk, T. Landefeld, E. Conte, K. Boulouchos, J. Czerwinski, *SAE Paper* 2004-2001-1270, 2004.
- [5] M.J. Castaldi, S. Etemed, W.C. Pfefferle, V. Khanna, K.O. Smith, *ASME* 127 (2005) 27–35.
- [6] C. Appel, J. Mantzaras, R. Schaeren, R. Bombach, A. Inauen, N. Tylli, M. Wolf, T. Griffin, D. Winkler, R. Carroni, *Proc. Combust. Inst.* 30 (2005) 2509–2517.
- [7] T. Griffin, D. Winkler, M. Wolf, C. Appel, J. Mantzaras, *ASME* 2004-54101, 2004.
- [8] S.S. Bharadwaj, L.D. Schmidt, *J. Catal.* 146 (1994) 11–21.
- [9] G.A. Deluga, J.R. Salge, L.D. Schmidt, X.E. Verykios, *Science* 303 (2004) 993–997.
- [10] B.J. Dreyer, I.C. Lee, J.J. Krumenacher, L.D. Schmidt, *IWCC6*, Ischia, Italy.
- [11] M. Reinke, J. Mantzaras, R. Bombach, S. Schenker, A. Inauen, *Combust. Flame* 141 (2005) 448–468.
- [12] M. Reinke, J. Mantzaras, R. Schaeren, R. Bombach, A. Inauen, S. Schenker, *Combust. Flame* 136 (2004) 217–240.
- [13] C. Appel, J. Mantzaras, R. Schaeren, et al., *Combust. Flame* 128 (2002) 340–368.
- [14] B. Steiner, *Raman spectroscopic investigation of turbulent premixed flames*, Dissertation, University of Stuttgart, 2002.
- [15] S. Eisenberg, *Raman Spectroscopy in a jet flame*, Diploma Thesis, University of Goettingen, 1995.
- [16] M. Schaefer, W. Ketterle, J. Wolfrum, *Appl. Phys. B* 52 (1991) 341–346.
- [17] W. Kang, O. Fujita, K. Ito, *ASME* 118 (1996) 82–87.
- [18] U. Dogwiler, P. Benz, J. Mantzaras, *Combust. Flame* 116 (1999) 243–258.
- [19] R. Schwiedernoch, S. Tischer, C. Correa, O. Deutschmann, *Chem. Eng. Sci.* 58 (2003) 633–642, available at <<http://www.detchem.com/mechanisms>>.
- [20] O. Deutschmann, L.I. Maier, U. Riedel, A.H. Stroemman, R.W. Dibble, *Catal. Today* 59 (2000) 141–150.
- [21] J. Warnatz, R.W. Dibble, U. Maas, *Combustion, Physical and Chemical Fundamentals, Modeling and Simulation*, Springer-Verlag, New York, 1996, available at <[http://reaflow.iwr.uni-heidelberg.de/ftp/reaflow/mechanism\\_for\\_export/Mech97.C1\\_C2\\_incl\\_thermodynamics](http://reaflow.iwr.uni-heidelberg.de/ftp/reaflow/mechanism_for_export/Mech97.C1_C2_incl_thermodynamics)>.
- [22] R.J. Kee, G. Dixon-Lewis, J. Warnatz, M.E. Coltrin, J.A. Miller, Report No. SAND86-8246, Sandia National Laboratories, 1996.
- [23] R.J. Kee, F.M. Rupley, J.A. Miller, Report No. SAND89-8009B, Sandia National Laboratories, 1996.
- [24] M.E. Coltrin, R.J. Kee, F.M. Rupley, Report No. SAND90-8003C, Sandia National Laboratories, 1996.
- [25] C. Appel, J. Mantzaras, R. Schaeren, R. Bombach, A. Inauen, *Combust. Flame* 140 (2005) 70–92.
- [26] A.G. Dietz III, L.D. Schmidt, *Catal. Lett.* 33 (1995) 15–29.
- [27] D.I. Shin, T. Dreier, J. Wolfrum, *Appl. Phys. B* 72 (2001) 257–261.

## Comment

Dimitrios Kyritsis, *University Illinois Urbana-Champaign, USA*. Would it be possible to perform this experiment using just a Nd-YAG laser and employing the second harmonic for Raman measurements and the third harmonic for formaldehyde LIF?

*Reply*. When using the third harmonic of the Nd-YAG laser at 355 nm for LIF, the recorded signal cannot be solely attributed to formaldehyde since the background contribution cannot be assessed. At rich operating conditions polycyclic aromatic hydrocarbons

(PAH) may also form, which have broad absorption and emission bands and contribute thus to the detected signal.

We have opted for a more complicated but rigorous approach (i.e., using a tunable laser), whereby subtracting the off-resonant from the on-resonant signal allowed for a realistic assessment of the formaldehyde LIF contribution.

Excitation wavelengths at 353 and 339 nm (well-known transitions of formaldehyde) have been investigated, and the former was chosen as it provided a more favorable signal-to-noise ratio. Even with the 352 nm excitation, the background contribution was still significant. Furthermore, a scan of the excitation wavelength indicated that the 355 nm radiation could not provide acceptable signal-to-noise ratio for our operating conditions.